*Biology of Reproduction*, 2019, 100(6), 1673–1685
doi:10.1093/biolre/ioz083
Research Article
Advance Access Publication Date: 14 May 2019



Research Article

# Non-canonical RNA polyadenylation polymerase FAM46C is essential for fastening sperm head and flagellum in mice†

**Chunwei Zheng[1,2], Ying-Chun Ouyang[1], Binjie Jiang[1], Xiwen Lin[1], Jian Chen[1], Ming-Zhe Dong[1], Xinjie Zhuang[3], Shuiqiao Yuan[4], Qing-Yuan Sun[1] and Chunsheng Han[1,2,*]**

[1]State Key Laboratory of Stem Cell and Reproductive Biology, Institute of Zoology, Chinese Academy of Sciences, Beijing, China; [2]University of Chinese Academy of Sciences, Savaid Medical School, Beijing, China; [3]Center for Reproductive Medicine, Peking University Third Hospital, Beijing, China and [4]Family Planning Research Institute, Tongji Medical College, Huazhong University of Science and Technology, Wuhan, Hubei, China

*__Correspondence__: Chunsheng Han, State Key Laboratory of Stem Cell and Reproductive Biology, Institute of Zoology, Chinese Academy of Sciences, Room D325, 1-5 Beichen West Road, Beijing, China 100101. Tel/Fax: 86-10-64807105; E-mail: hancs@ioz.ac.cn

†__Grant Support:__ This work was supported by grants from the Ministry of Science and Technology of China (2015CB943002, 2016YFC1000606), the National Natural Science Foundation of China (31771631, 81671513), and the Beijing Natural Science Foundation (7172236). All of the sequence data are available in GEO under the accession number GSE124233.
Edited by Dr. Monika A. Ward, PhD, University of Hawaii John A. Burns School of Medicine

Received 3 January 2019; Revised 24 March 2019; Accepted 13 May 2019

## Abstract

Family with sequence similarity 46, member C (FAM46C) is a highly conserved non-canonical RNA polyadenylation polymerase that is abundantly expressed in human and mouse testes and is frequently mutated in patients with multiple myeloma. However, its physiological role remains largely unknown. In this study, we found that FAM46C is specifically localized to the manchette of spermatids in mouse testes, a transient microtubule-based structure mainly involved in nuclear shaping and intra-flagellar protein traffic. Gene knockout of FAM46C in mice resulted in male sterility, characterized by the production of headless spermatozoa in testes. Sperm heads were intermittently found in the epididymides of FAM46C knockout mice, but their fertilization ability was severely compromised based on the results of intracytoplasmic sperm injection assays. Interestingly, our RNA-sequencing analyses of FAM46C knockout testes revealed that mRNA levels of only nine genes were significantly altered compared to wild-type ones ($q < 0.05$). When considering alternate activities for FAM46C, in vitro assays demonstrated that FAM46C does not exhibit protein kinase or AMPylation activity against general substrates. Together, our data show that FAM46C in spermatids is a novel component in fastening the sperm head and flagellum.

## Summary Sentence

Non-canonical RNA polyadenylation enzyme FAM46C is specifically expressed in the manchette of spermatids in mouse testes and plays an essential role in spermiogenesis by fastening the sperm head and tail together.

**Key words:** male infertility, spermatogenesis, intracytoplasmic sperm injection (ICSI).

## Introduction

A recently recognized prominent feature of spermatogenesis is the generation and dynamic changes of highly diversified RNA species in various spermatogenic cells [1]. These diverse transcripts are a result of alternative transcription initiation, polyadenylation, splicing, and other RNA processing and metabolizing steps, which are all regulated by various RNA binding proteins (RBPs). Indeed, it is well established that several key regulators of spermatogenesis are RBPs [2]. The human genome contains more than 1500 RBP genes, and the testis ranks the highest in terms of the number of tissue-specific RBPs [3]. However, few RBPs with defined functions in spermatogenesis have been identified, and mechanistically these proteins are poorly understood. In search of novel RBPs with potential functions in spermatogenesis, we found that FAM46C, a non-canonical polyadenylation polymerase, is a promising candidate because it is highly expressed in the mouse and human testis and is involved in tumorigenesis.

FAM46C deletions and mutations are frequently identified in the tumor samples of multiple myeloma patients [4, 5] and are strongly associated with poor prognosis [6]. More than 70 somatic mutations across the whole FAM46C gene, many of which are frameshift or nonsense mutations, have been identified [7]. Previous studies reported variant allele frequencies ranging from 3.8–100% dependent on samples. Two recent studies show that FAM46C mutations are associated with myeloma pathogenesis and progression via perturbation in plasma cell survival and differentiation [8, 9]. FAM46C has also been reported to serve as a biomarker of hepatic recurrence in patients with gastric cancer [10] and to mediate the antimetastatic effects of norcantharidin on hepatocellular carcinoma cells [11, 12]. There is no information about the fertility of the patients.

Based on RNA-sequencing (RNA-seq) data from 27 human tissues, human FAM46C mRNA levels are most abundant in bone marrow, followed sequentially by testis, stomach, colon, bladder, and lymph node [13]. In mice, FAM46C transcript levels are most abundant in adult testis, followed by fetal liver and adult spleen according to RNA-seq data published by the Mouse ENCODE Consortium [14]. Our previously published RNA-seq data on mouse testicular cells revealed that FAM46C is abundantly expressed in mouse haploid cells [15].

FAM46C is predicted to be a novel member of the nucleotidyltransferase (NTase) fold superfamily, which includes the RNA polyadenylation polymerase and protein AMPylation enzyme subfamilies [16, 17]. Nucleotidyltransferase fold proteins transfer nucleoside monophosphate from nucleoside triphosphate to a hydroxyl group in proteins, nucleic acids, or small molecules. Proteins from this superfamily are involved in many important biological processes, such as RNA polyadenylation, RNA editing, DNA repair, protein modification, and antibiotic resistance. Both humans and mice have four FAM46 members (FAM46A, B, C, and D) that constitute a small family of conserved NTase fold proteins. Sequence identity between mice and human FAM46C is 96%. The RNA polyadenylation polymerase activity of FAM46C was recently confirmed by in vitro assays using its recombinant proteins [9].

Based on these features, we proposed that FAM46C might play an essential role in spermatogenesis by acting as an RNA polyadenylation polymerase or through another type of NTase activity. We generated FLAG-FAM46C knockin (KI) and FAM46C knockout (KO) mice to investigate its expression and physiological role in spermatogenesis, respectively. We also tested whether FAM46C might act as a protein kinase or AMPylator using in vitro assays. Our data showed that FAM46C in mouse testes is only detected in the manchette, a specialized structure in spermatids, and FAM46C KO male mice display complete sterility due to the production of acephalic sperm. Moreover, we found that FAM46C does not exhibit any detectable protein kinase or AMPylation activity to general substrates. Collectively, our results indicate that a major function of the evolutionarily conserved FAM46C in mice is to fasten the sperm head and flagellum during spermiogenesis.

## Materials and methods

### Mice

All animals used in this study were bred by following the guidelines of the Animal Care and Use Committee of the Institute of Zoology, Chinese Academy of Sciences. All procedures were conducted by following the institutional guidelines and in accordance with SSR's specific guidance and standards.

To generate KO mice using the CRISPR-Cas9 technology, Cas9 mRNAs and sgRNAs were in vitro transcribed from pST1374-Cas9-N-NLS-flag-linker (product no. 44 758; Addgene) and pUC57-sgRNA (product no. 51 132; Addgene) expression vectors, respectively, by following the procedures described by Shen et al. [18]. Sequences of sgRNA oligos are listed in Supplementary Table S1. Cas9 mRNA (100 ng/$\mu$l) and sgRNAs (50 ng/$\mu$l each) were injected into the cytoplasm of zygotes obtained by mating DBA males with superovulated C57BL/6J females. We generated two male founder mice: one had a 39-bp deletion in the second exon and the other contained a single-base deletion at + 232 bp of the coding sequence. The first founder was crossed with C57BL/6J female mice for further breeding while the second one was crossed with ICR females. The primers used in genotyping are also listed in Supplementary Table S1.

### Isolation of testicular cells by gravity sedimentation

Testicular cells were isolated by following a protocol previously published by us [19]. Briefly, total testicular cells were harvested by digesting the testes using collagenase (1 mg/ml, 5 min, 37°C) and trypsin (0.25%, 5 min, 37°C) after removal of the albuginea. Dispersed cells were suspended in DMEM medium (product no. 11 965–092; GIBCO) with 0.5% BSA (product no. a9647; Sigma), and then loaded into a glass cylinder on top of 600 ml of BSA solution of 2–4% BSA gradient in DMEM. After 3 h of sedimentation, the cell fractions were collected from the bottom of the cylinder. Different types of cells were isolated from mice of different ages as the following: Sertoli cells (Sertoli) from 6-dpp mice, preleptotene spermatocytes (plpSC), and pachytene spermatocytes (pacSC) from 17-dpp mice, and round spermatids (rST) and elongating spermatids (eST) from 60-dpp adult mice. The purity of each cell type was confirmed by quantitative real-time reverse transcription polymerase chain reaction (RT-PCR) assessment of their marker genes (Supplemental Figure S1). Primer sequences are listed in Supplementary Table S1.

### Real-time RT-PCR

Total RNAs were extracted using Trizol (product no. 15 596–026; Invitrogen) by following the manufacturer's protocol. Reverse transcription was performed using Reverse Transcription System (product no. G3250; Promega) according to the standard protocol. Real-time PCRs were performed using UltraSYBR Mixture (product

no. 11201ES08; Yeasen Biotech) on a LightCycler 480 platform (Roche Diagnostics). Expression values were calculated using the ΔΔCt method with *β-Actin* as the internal control. Primer sequences are listed in Supplementary Table S1.

### Validation of FLAG-FAM46C KI mice by western blotting

Haploid cells were fluorescence-activated cell sorting (FACS) sorted from total testicular cells from 6-month wild-type (WT) and KI mice stained with Hoechst dye. Cell lysates were prepared using (radioimmunoprecipitation assay) RIPA buffer (product no. P0013B; Beyotime Biotechnology) supplemented with Protease Inhibitor Cocktail (product no. P8340; Sigma). The proteins were separated by SDS-PAGE and then electrotransferred onto a nitrocellulose membrane. Antibody incubation and washing were conducted using standard protocols. Antibodies and their dilutions are listed in Supplementary Table S2. Images were recorded using the ChemiDoc XRS$^+$ system (Bio-Rad).

### Fertility tests

The fertility tests were carried out by mating adult F2 male mice with adult WT female mice. For FAM46C-39, six male mice for each of the three genotypes (WT, heterozygous (Het), and KO) were tested. For FAM46C-1, three male mice for each of the two genotypes (WT and KO) were tested. One F2 male was caged with two WT ICR females for 3 months and total number of offspring of each male mouse was divided by the number of litters to give the average litter size, which was further averaged as each male mouse were tested.

### Computer-assisted sperm analysis (CASA)

The sperm motility assays were performed by following a protocol described by Chen et al. [20]. Briefly, a cauda epididymis was dissected from adult mice and placed in 1 ml pre-warmed (37°C) HTF medium (product no. MR-070-D; Millipore). The epididymis was squeezed using forceps and was incubated at 37°C for 30 min in a 5% $CO_2$-containing incubator to allow sperm release. Sperm motility was analyzed using the CASA system (product no. Version.12 CEROS; Hamilton Thorne Research).

### Immunofluorescence

Testes were dissected immediately after the animals were killed, fixed in 4% paraformaldehyde (PFA) at 4°C for 24 h, and then embedded in paraffin after dehydration in ethanol. The 5-μm sections were prepared. Deparaffinized sections were incubated in sodium citrate buffer (product no. ZLI-9065; ZSGB-BIO) at 95°C for 15 min and blocked with 5% BSA. The primary antibody was added and the sections were kept at 4°C overnight, followed by incubation with the secondary antibody at room temperature. Subsequently, rhodamine-labeled peanut agglutinin (PNA) (product no. RL-1072; Vectorlabs) was used to label the acrosome. Briefly, the original PNA solution was first diluted at 1:200 with 5% BSA and added to the secondary antibody-treated slides for 30 min at room temperature. The slides were then briefly rinsed using PBS (137.0 mM NaCl, 2.7 mM KCl, 10.1 mM $Na_2HPO_4$, 1.8 mM $KH_2PO_4$). The nuclei were stained with 4, 6-diamidino-2-phenylindole (DAPI) (product no. C1002; Beyotime Biotechnology) at room temperature for 5 min. Antibodies and their dilutions are listed in Supplementary Table S2.

### Hematoxylin and eosin (HE) staining

For staining of testis sections, mouse testes were fixed in Bouin's solution (product no. BRY-1973; BioRoYee) at 4°C for 24 h and paraffin-embedded after dehydration with ethanol. The 5-μm sections were prepared. Hematoxylin and eosin staining was carried out by following the standard protocol. Briefly, after deparaffinization, sections were stained with hematoxylin for 1 min, rinsed in 50%, 70%, and 80% ethanol, and then stained with eosin for 1 min and rinsed in 90%, 100% ethanol, and 100% xylene. The coverslip was then mounted.

For staining of sperm, a drop containing 10 μl of sperm prepared from the epididymis was dried on a slide, fixed in 4% PFA for 15 min, and then rehydrated in $H_2O$ for 5 min. Sperm were stained with hematoxylin for 2 min, sequentially rinsed in $H_2O$ and in 50%, 70%, and 80% ethanol. Sperm were then stained with eosin for 1 min and rinsed in 90%, 100% ethanol, and 100% xylene. The coverslip was then mounted.

### TUNEL assays

TUNEL assays on paraffin-embedded sections were performed by using the DeadEnd Fluorometric TUNEL system and following the manufacturer's protocol (product no. G3250; Promega). For co-staining of Wilms tumor 1 homolog (WT1) and TUNEL, paraffin-embedded sections that had been subjected to the whole process of WT1 immunostaining were digested by proteinase K followed by the remaining steps of the TUNEL assay.

### Transmission electron microscopy

Adult testes were fixed with a solution containing 1.5% glutaraldehyde, 1.5% PFA and 0.2% picric acid in 0.2 M phosphate buffer (PB) (product no. 211 544; BD) overnight at 4°C. The tissues were washed in 0.1 M PB, cut into small pieces and post-fixed in 1% $OsO_4$ in 0.1 M PB for 2 h at 4°C. The samples were dehydrated using 30%, 50%, 75%, 95%, and 100% ethanol sequentially and embedded in resin. Ultrathin sections of 60–70 nm were stained with uranyl acetate and lead citrate. Images were taken using a JEM-1400 transmission electron microscope (JEOL). As some structures could be missed depending on the position and/or angle of sectioning, we selected images that displayed both normal nuclear structure and at least a portion of the tail proximal to the nucleus, and then counted the connecting pieces with incomplete capitulum and/or segmented columns to produce the quantitative results.

### RNA-sequencing analyses

Total RNAs were extracted from testes of two WT and two KO adult mice using Trizol (product no. 15 596–026; Invitrogen). High-throughput sequencing libraries were constructed using the NEBNext Ultra RNA Library Prep Kit for Illumina. Sequencing was performed on the Illumina HiSeq X10 platform (Novogene). The sequencing reads were mapped to the mouse genome (UCSC mm9) with TopHat (v2.0.6). The mRNA expression levels were represented by fragments per kilobase of transcript sequence per millions (FPKM) calculated by Cufflinks (v2.0.2). The differentially expressed genes were identified with the Cuffdiff package based on the threshold of q-value ($q < 0.05$).

### Purification of recombinant proteins

Purification of GST-VopSΔ30 was performed as previously described [21]. Purification of 6xHIS-Rac1V12 was performed as

previously described [22]. For purification of FAM46C, a plasmid for expression of 6xHis- FAM46C was transformed into Rosetta cells, grown to mid-log phase (A600∼0.5), and induced with 100 $\mu$M Isopropyl $\beta$-D-1-thiogalactopyranoside at 20°C for 16 h. Cells were lysed using a cell disrupter (Emulsiflex-C3) and proteins were purified using a standard nickel-affinity purification protocol (Thermo Scientific).

### In vitro AMPylation and phosphorylation of recombinant proteins

In vitro AMPylation and phosphorylation assays were performed as follows. Recombinant 6xHIS-Rac1V12, $\beta$-Casein (Sigma-Aldrich), Mylein Basic Protein (Sigma-Aldrich), and Histone H4 (New England Biolabs) were used as substrates (1 $\mu$M) for the enzymes 6xHIS-FAM46C (400 nM), GST-VopSΔ30 (20 nM), and Casein Kinase II (20 units) (New England Biolabs). Reactions were performed in reaction buffer (25 mM HEPES-KOH, pH 7.4, 100 mM KCl, 8 mM $MgCl_2$, 1 mM $CaCl_2$, 0.1% Triton) supplemented with 250 mM cold ATP and either ∼0.5 $\mu$Ci of [$\alpha^{32}$P]ATP or [$\gamma^{32}$P]ATP at 30°C for 30 min. Samples were analyzed by SDS-PAGE, stained with Coomassie Brilliant Blue, and dried. The [$^{32}$P] radioactive signal was detected with a Typhoon FLA 7000 (GE) upon ∼18 h exposure using Storage Phosphor Screens.

### Intracytoplasmic sperm injection assays (ICSI)

Intact sperm from WT mice and a mixture of sperm, sperm heads, and tails from KO mice were collected from caudal epididymis and efferent duct by gentle squeezing with forceps in HTF medium (product no. MR-070-D, Millipore), and were sonicated to dissociate heads from tails with a sonicator (Kontes). Sonication was carried out in such a way (four pulses of 10 s each) that about 70% sperm from WT mice have their heads and tails dissociated. Sperm heads were collected by centrifugation in 70% Percoll (product no. P4937; Sigma), and injected into WT oocytes obtained from superovulated 8-week-old ICR female mice. Injected oocytes were transferred to KSOM medium (product no. MR-107-D, Millipore) and cultured at 37°C, with 5% $CO_2$. After 5–8 h the injected oocytes developed to the pronucleus stage and were transferred into pseudo-pregnant ICR females. Offspring were examined 20 days after embryo transfer, and genotyped by sequencing the PCR-amplified FAM46C locus where the deletion mutation occurred.

### Data analyses and statistics

Statistical significance was evaluated using a *t* test. Results are presented as mean ± SD. The data were considered significant with *P* value was less than 0.05 (*), 0.01 (**), or 0.001 (***). All of the experiments were independently repeated at least three times.

## Results

### FAM46C is localized to the manchette of spermatids in mice

FAM46C is highly conserved in metazoans (Supplemental Figure S2). We used RT-PCR to detect FAM46C expression and found that it was most abundantly expressed in the testis and the spleen among eight organs of adult mice (Figure 1A), consistent with previously published RNA-seq data [14]. Using quantitative RT-PCR analyses, we found that FAM46C mRNA was much more abundant in round and elongating spermatids than in other testicular cell types (Figure 1B), supporting our previously published RNA-seq results [15]. We used the CRISPR-Cas9 technique to insert an in-frame, N-terminal FLAG-tag for FAM46C in mice (Figure 1C). A region spanning the KI site was PCR-amplified and sequenced to validate the KI of the FLAG-encoding sequence to the FAM46C gene locus. We conducted western blotting analyses on haploid spermatogenic cells of WT and KI mice, and we confirmed that FLAG-FAM46C is expressed in the KI but not the WT mice (Figure 1D). New generations of KI mice were sired by either homozygous or Het males, of which the litter sizes were 10.7 and 11, respectively, not significantly different (Supplemental Figure S3A). Furthermore, no defect was seen on the HE-stained epididymal sections and the epididymal sperm of the homozygous male mice compared with the WT counterparts (Supplemental Figure S3B and C).

Using a monoclonal anti-FLAG antibody (anti-FLAG) in immunofluorescence assays on the adult testis sections of FLAG-FAM46C mice, we observed a cap-like structure on one side of step eight elongating spermatids (Figure 1E). The cap-like structure was opposite to the acrosome revealed by rhodamine- PNA staining [23], and extended to become a girdle-like structure concurrent with nuclear condensation and elongation as spermatids progress from step 8–14. The FLAG staining appeared to disappear in step 15–16 spermatids (Figure 1E). The dynamic localization pattern of FLAG-FAM46C matches that of the manchette, a microtubular platform that is transiently formed in the perinuclear region of spermatids between step 8 and 14 and that is involved in vesicle transport and spermatid head re-shaping [24]. Furthermore, we carried out pair-wise co-immunostainings of LAMIN B1, which is a protein localized to the nuclear lamina to the posterior nuclear pole of the late step round spermatids, $\alpha$-TUBULIN, and FLAG-FAM46C (Fig. 1F). The stainings of LAMIN B1 and $\alpha$-TUBULIN were observed at inner and outer layers surrounding the DAPI-stained nuclei of step 8 spermatids, respectively. Similar non-overlapping localizations of LAMIN B1 and FLAG-FAM46C were also observed. In contrast, FLAG-FAM46C and $\alpha$-TUBULIN were always observed to be localized to the same layer. Together, these results showed that FAM46C is specifically expressed in spermatids from step 8–14 and localizes to the manchette (Figure 1G).

### FAM46C is required for male fertility in mice

To determine the physiological function of FAM46C in testes, we generated FAM46C KO mice using the CRISPR/Cas9 technique. Two male founder mice were generated. The first contained a mutant allele corresponding to a deletion of 13 amino acids (aa 68–80) close to the N-terminus of the NTase domain of FAM46C (FAM46C-39) and the second had a mutant allele with a single-base deletion at +232 bp of the coding sequence (FAM46C-1), resulting in a frameshift after aa 77 and a truncated protein at aa 92 (Supplemental Figure S4A and B). These founder mice were crossed with WT females to generate F1 offspring, which were further crossed to produce F2 mice for phenotypic evaluation (Supplemental Figure S4C). For the offspring of the FAM46C-39 founder, the WT, Het, and KO littermates were identified by genomic PCRs (Supplemental Figure S4D). The genotyping of the FAM46C-1 offspring was conducted by sequencing the PCR-amplified mutant allele. As the genotyping of the mice containing the FAM46C-39 allele was easier, we focused on the FAM46C-39 mice including KO, Het mice, and their WT littermates for further study unless otherwise described.

Neither Het nor KO mice were different from the WT littermates in terms of appearance or behavior regardless of age and sex. However, we detected several hematologic abnormalities in FAM46C KO

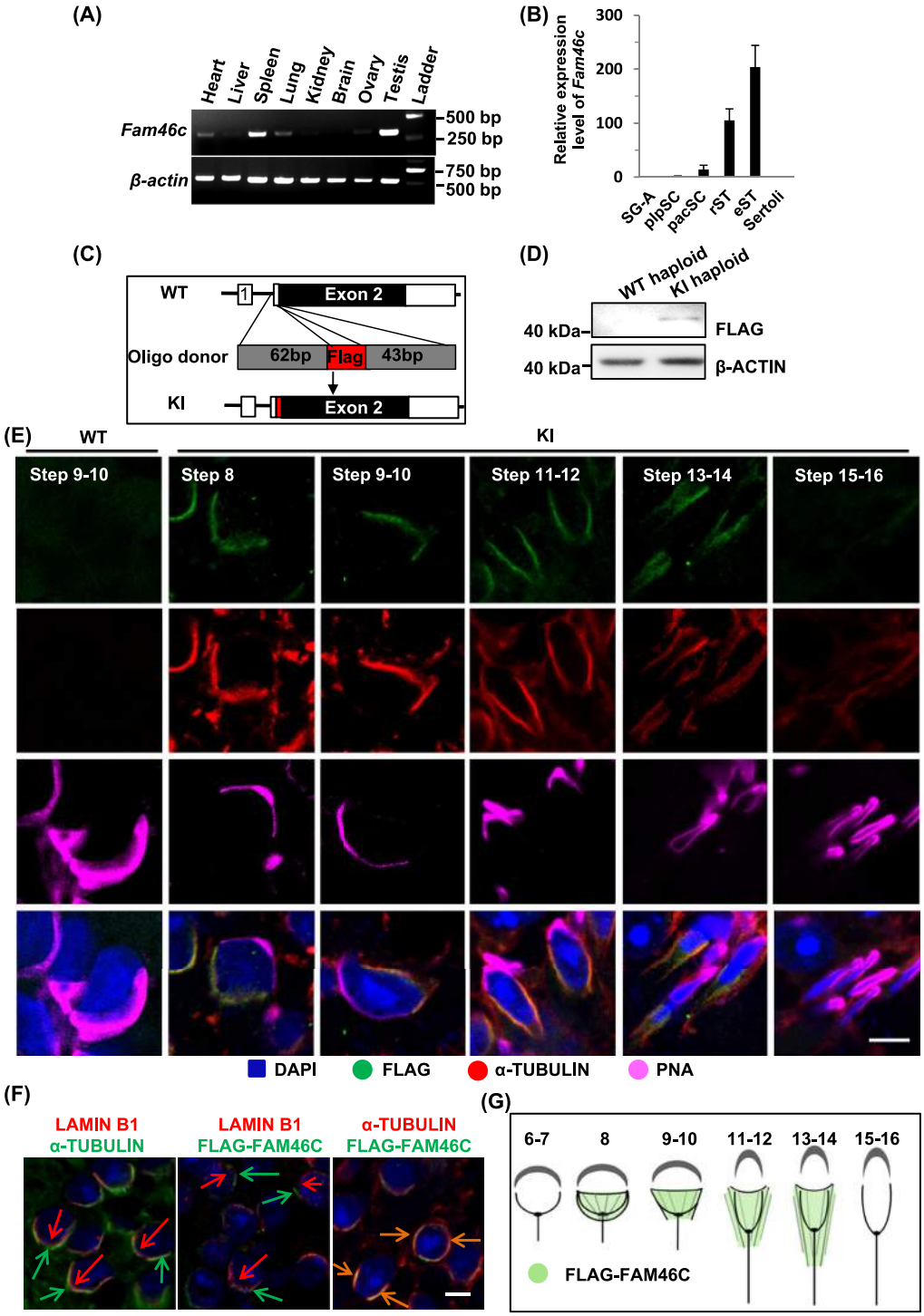


**Figure 1.** FAM46C is localized to the manchette of spermatids. **(A)** RT-PCR analyses of FAM46C mRNA expression in multiple organs of mice. **(B)** Quantitative RT-PCR analyses of FAM46C mRNA abundance in testicular cells. SG-A, type A spermatogonia; plpSC, preleptotene spermatocytes; pacSC, pachytene spermatocytes; rST, round spermatids; eST, elongating spermatids; Sertoli, Sertoli cells. The expression values in different cells were normalized by the SG-A value. (n = 3). **(C)** A schematic illustration of the CRISPR-Cas9-generated KI of the FLAG-encoding sequence in the genomic locus to produce a gene that encodes FAM46C with a FLAG tag at the N-terminus. **(D)** Validation of the KI mouse model. Haploid cells were sorted from 6-month-old WT and KI mice stained with Hoechst dye using FACS. Western blotting analyses on haploid lysates of WT and KI mice showing that FLAG-FAM46C is detected in the haploid cells of the KI mice. **(E)** Immunofluorescent localization of FLAG-FAM46C to the manchette in spermatids from step 8–16. Testis sections from FLAG- FAM46C KI mice were immunostained with anti-FLAG antibody, anti-$\alpha$-TUBULIN antibody. The acrosome was stained with rhodamine-PNA. Immunostaining of WT testis sections with anti-FLAG antibody was used as negative control for the FLAG-FAM46C signals in KI mice; immunostaining of WT sections without primary antibody was used as a negative control for the $\alpha$-TUBULIN immunostaining. Bars = 5 $\mu$m. **(F)** Pair-wise co-immunostainings of LAMIN B1, $\alpha$-TUBULIN, and FLAG-FAM46C. Green and red arrows indicate the non-overlapping localization of LAMIN B1 and $\alpha$-TUBULIN and that of LAMIN B1 and FLAG-FAM46C; orange arrows show the co-localization of FLAG-FAM46C and $\alpha$-TUBULIN. Bars = 5 $\mu$m. **(G)** Schematic summary of FAM46C localization in the manchette of mouse spermatids at different steps.

mice such as lower levels of hemoglobin, hematocrit, mean corpuscular volume, mean corpuscular hemoglobin, and mean corpuscular hemoglobin concentration, as well as increased levels of red blood cells and blood platelets (Supplemental Figure S4E–L), consistent with a recent study by Mroczek et al. [9].

The size and morphology of the KO testes were comparable to those of the WT by visual inspection (Figure 2A). Quantitative analyses showed that WT, Het, and KO mice had the same body and testis weight (Supplemental Figure S5A and B). Surprisingly, FAM46C KO male mice were completely infertile (Figure 2B). We counted epididymal sperm and found that their number in KO mice was about 50% of that in WT mice (Figure 2C). CASA revealed that the numbers of swimming sperm of the KO mice regardless of the speed were significantly lower than those of the WT mice, while the number of static ones in FAM46C KO mice was higher than that of the WT mice (Figure 2D). No apparent defect was seen in the testis sections of the KO and WT littermates in terms of the cell types, cell morphology, and acrosome formation (Figure 2E; Supplemental Figure S5C and D). However, HE staining of the epididymides of the KO mice revealed loss of discernable nuclei (Figure 2F). Similar observations on the lack of nuclear staining in epididymal sperm and infertility were made for the FAM46C-1 KO mice (Supplemental Figure S5E–G). Thus, these data indicate that FAM46C is essential for male fertility and may function during spermiogenesis in mice.

## Sperm from FAM46C KO mice are acephalic

To define the underlying causes of male infertility in FAM46C KO mice, we collected and diluted "sperm" from the epididymides of KO mice for closer examination. Using HE-staining, we found that the FAM46C KO "sperm" was actually just composed of flagellum (Figure 2G). Occasionally, tailless heads positively stained by hematoxylin and whole sperm were observed, but their proportions were much lower than that of headless tails (Figure 2G). Similarly, sperm from the FAM46C-1 KO mice were almost all headless (Supplemental Figure S5H). These rare sperm heads were morphologically indistinguishable from those of the WT sperm based on HE-staining (Supplemental Figure S6A). Furthermore, the bare heads found in the epididymides, similar to the WT sperm, were positively stained with both DAPI and an antibody against SP56 (also known as zona pellucida 3 receptor, ZP3R), a component of the acrosome, while the negatively stained acephalic sperm were just flagella (Figure 2H). We re-examined the sperm in the epididymides by co-immunostaining of DNA with DAPI and the flagella with an $\alpha$-TUBULIN antibody. Sperm in WT epididymides were double positive for DNA and $\alpha$-TUBULIN staining while sperm in FAM46C KO epididymides were mainly positive for $\alpha$-TUBULIN with DAPI signals occasionally seen for loose heads (Supplemental Figure S6B).

Since the epididymides were almost exclusively filled with flagella, we postulated that the head-tail detachment of KO sperm occurred in the testis before the disengagement of sperm heads from the Sertoli cells. TUNEL assay showed that many apoptotic nuclei were observed in FAM46C KO but not WT sections, and about 13% of the KO tubules contained apoptotic signals (Figure 2I). Interestingly, the positive foci were adjacent to the base membrane of the stages VII–VIII seminiferous tubules rather than in their adluminal compartment (Figure 2I), which was confirmed by periodic acid-Schiff (PAS) staining and transmission electron microscope (TEM) images (Supplemental Figure S7A and B). We carried out a co-immunostaining of TUNEL and WT1, a specific marker of Sertoli cells in the testis, to show that the two signals do not colocalize but are close to each other, suggesting that the apoptotic nuclei and the Sertoli cell nuclei are both inside Sertoli cells (Supplemental Figure S7C). We also found that both the morphology and the number of WT1-positive Sertoli cell nuclei were indistinguishable in WT and KO mice (Supplemental Figure S7D). These results suggested that the apoptotic nuclei represented spermatids engulfed by Sertoli cells.

## The connecting piece can form but disassembles in FAM46C KO mice

As FAM46C is localized to the manchette of spermatids, we next examined whether manchette formation or morphogenesis during spermatogenesis was disrupted in KO mice. In both WT and KO mice, the manchette structures of spermatids from step 8–14 were clearly visualized by $\alpha$-TUBULIN immunostaining, and no difference was seen between KO and WT mice (Figure 3A). TEM images showed that the ultrastructure of manchette was the same in KO and WT mice (Figure 3B). Moreover, no defect was detected in the flagellar structure of the KO mice based on TEM images of flagellar cross sections and the typical "9 + 2" microtubular structure was readily seen in the midpiece, principal piece, and end piece of the flagella (Figure 3C).

We next focused on examining the structure of the connecting piece, a structure that plays a critical role in anchoring the sperm tail to the head. The connecting piece starts to form around the two centrioles in round spermatids and consists of nine segmented columns with their cranial ends fused to form a curved plate-like disk named capitulum and their caudal ends attached to the outer dense fiber of the flagellum [25]. The capitulum links the connecting piece to the outer nuclear membrane at the attachment site known as the implantation fossa. From TEM images of both WT and FAM46C KO testis sections, we observed that the proximal centrioles and segmented columns were located adjacent to the nucleus opposite to the forming acrosome in step 7–8 spermatids (Figure 3D). From step 10–12, the connecting piece developed further, and more recognizable segmented columns were observed in both WT and KO spermatids. However, from step 13–16, incomplete segmented column and/or capitulum were observed in 90% (43 out of 48) of the connecting pieces of FAM46C KO mice. In contrast, only 10% (2 out of 21) of abnormal connecting pieces were observed in WT mice.

## FAM46C has no AMPylation or protein kinase activity for general substrates

We conducted RNA-seq analyses to profile and compare the transcriptomes of WT and KO mice but found only nine genes that changed their transcript levels ($q < 0.05$; Supplementary Table S3), namely: insulin-like 3 (*Insl3*), 3 beta- and steroid delta-isomerase 6 (*Hsd3b6*), lipocalin 2 (*Lcn2*), hemoglobin, beta adult s chain (*Hbb-bs*), complement component 3 (*C3*), angiotensinogen (*Agt*), actin-binding Rho activating protein (*Abra*), glutathione peroxidase 3 (*Gpx3*), and kallikrein 1-related peptidase b21 (*Klk1b21*). These genes are not functionally related, particularly in spermatogenesis. This observation, together with the fact that FAM46C was localized in the manchette of the elongating spermatids instead of in their nuclei, strongly suggested that FAM46C was unlikely to function as an RNA polyadenylation polymerase. We next set out to determine if FAM46C had in vitro AMPylation or protein kinase activity. We first purified recombinant FAM46C and tested its ability to AMPylate or phosphorylate commonly used generic substrates. For these assays, recombinant FAM46C, VopS (AMPylation positive control), and Casein Kinase II (kinase positive control) were

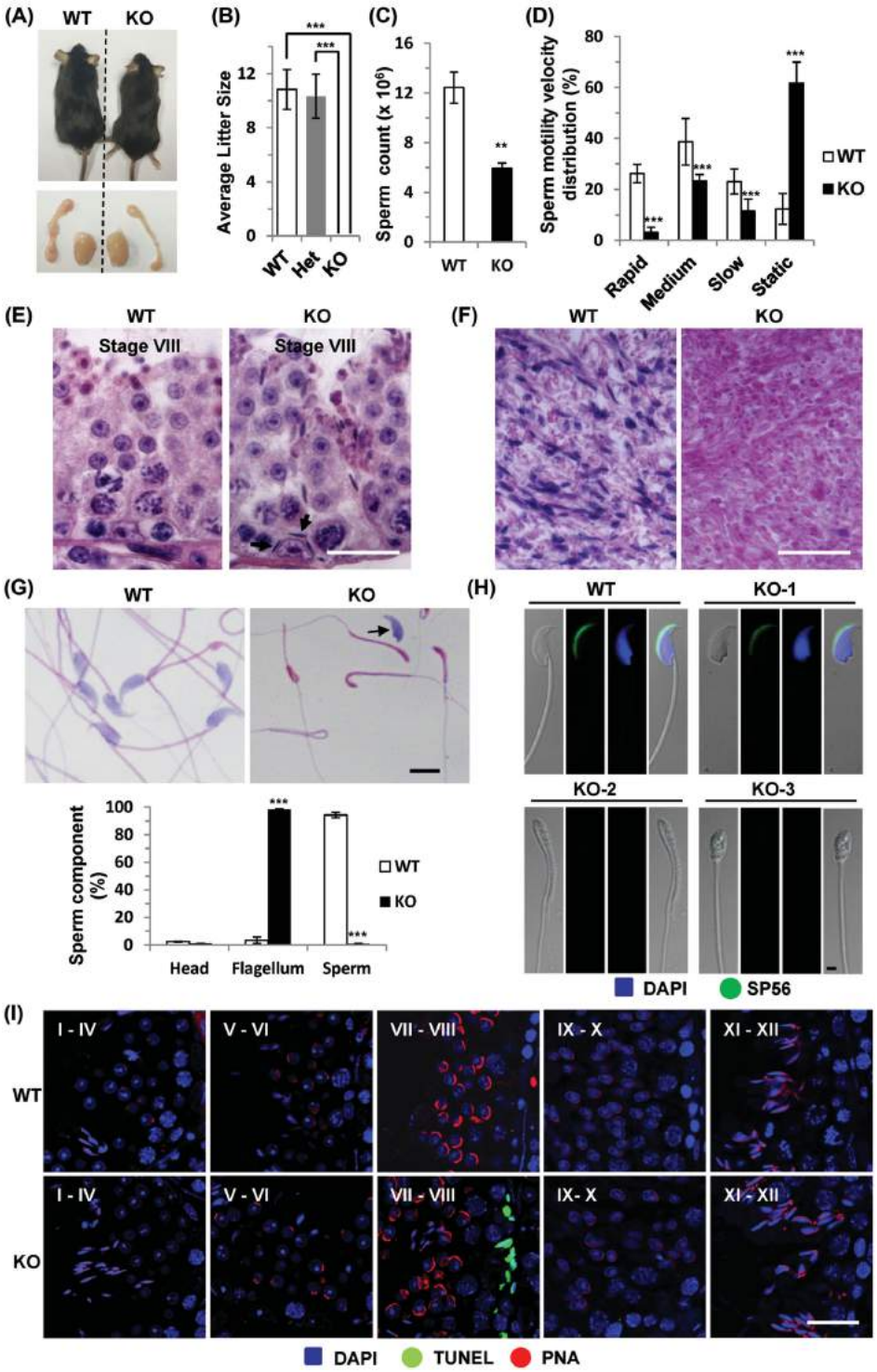


**Figure 2.** Inactivation of FAM46C results in acephalic sperm. **(A)** Pictures of WT and KO mice and their testis and epididymis. **(B)** Litter sizes of WT, Het, KO male mice. (n = 6). **(C)** The epididymal sperm counts of WT and FAM46C KO mice based on the flagellum. Total sperm/sperm flagella were collected from the epididymides and counted using a hematocyte counter. (n = 4). **(D)** Motility assessment of WT and KO sperm/sperm flagella collected from the epididymis using CASA. (n = 5). **(E-F)** Histological analyses of the testis **(E)** and epididymis **(F)** sections from WT and FAM46C KO mice stained with HE. Black arrows, sperm heads localized in the basal compartment of the seminiferous tubules. Bars = 10 $\mu$m. **(G)** HE staining of sperm released from epididymis showing that KO sperm are acephalic. Note that heads and tails of WT sperm were stained by HE, respectively, while the KO sperm were only stained positive by eosin, indicating that they were acephalic. Occasionally, hematoxylin-positive sperm heads (black arrow) were observed in KO samples. Bars = 5 $\mu$m. The percentages of different components of sperm from caudal epididymides of WT and FAM46C KO mice. (n = 4). **(H)** Characterization of loose heads and tails of KO sperm released from epididymides using immunofluorescent staining of acrosome and DNA. Note that WT sperm and KO sperm heads (KO-1) were double positive for acrosome marker SP56 and DNA DAPI staining, respectively. The sperm tails with different morphologies (KO-2 and KO-3) were negatively stained. Bars = 2 $\mu$m. **(I)** TUNEL staining of testis sections from WT and KO mice. KO but not WT seminiferous tubules at stage VII–VIII of the seminiferous cycle contained many TUNEL-positive nuclei close to the base membrane. Bars = 25 $\mu$m.

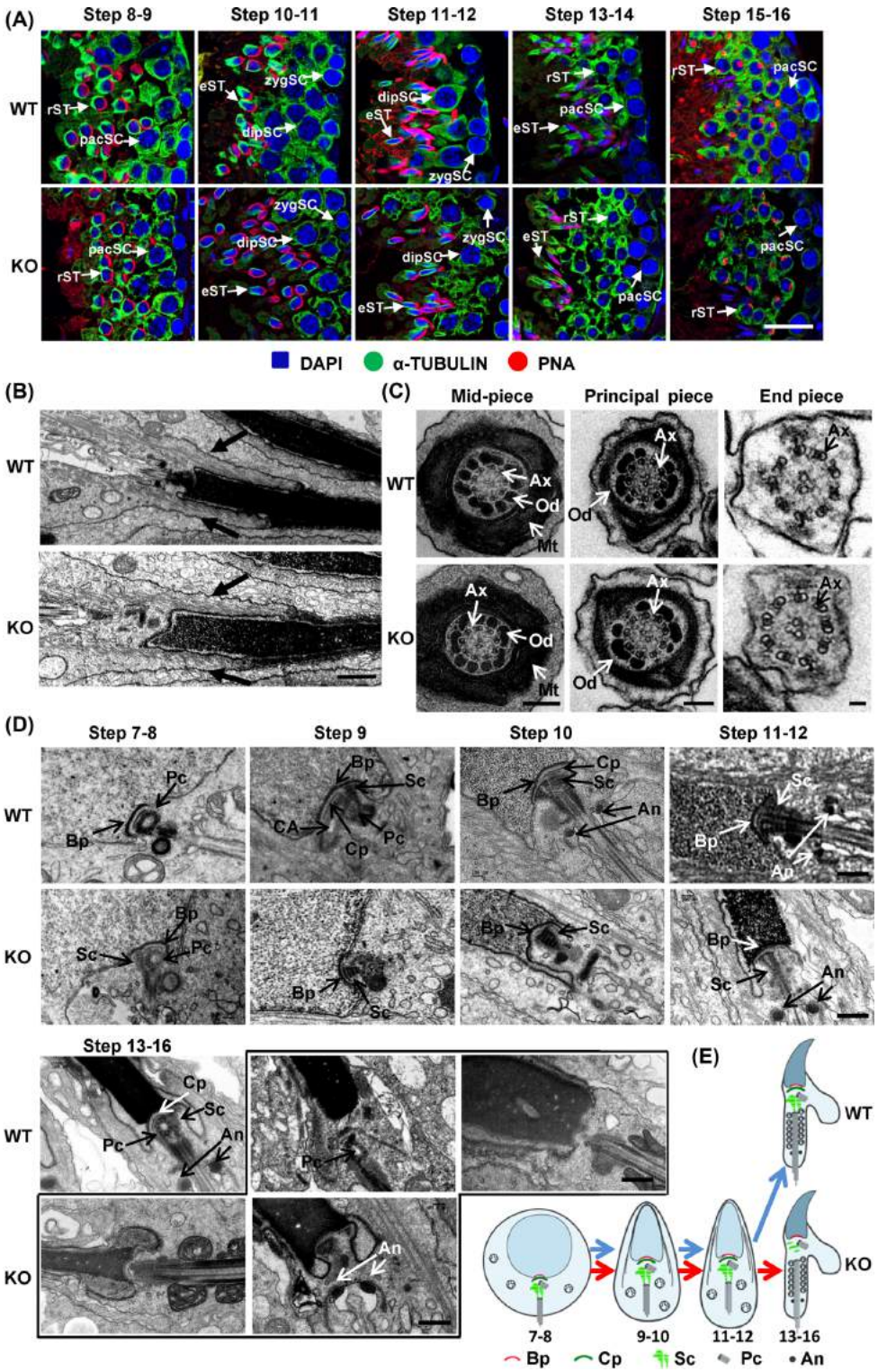


**Figure 3.** FAM46C KO leads to disassembly of the connecting piece of the flagellum. **(A)** Comparison of manchette morphogenesis between KO and WT spermatids. The manchette structure was revealed by the immunostaining of $\alpha$-TUBULIN. The acrosome was stained with rhodamine-PNA. zygSC, zygotene spermatocyte (SC); pacSC, pachytene SC; dipSC, diplotene SC; rST, round spermatid (ST); eST, elongating ST. bars = 25 $\mu$m. **(B)** TEM images showing the manchette (black arrows) in WT and FAM46C KO mice. Bars = 1 $\mu$m. **(C)** TEM images of the cross-sections of the mid-piece, the principal piece and the end piece of WT and FAM46C KO sperm flagellum. Mt, mitochondria; Ax, axoneme; Od, outer dense fiber. Bars = 200 nm. **(D)** TEM analyses of connecting piece dynamics. The forming and well-formed connecting pieces with recognizable segmented column (Sc), proximal centriole (Pc) and capitulum (Cp) were seen in spermatids from step 7–12 in both WT and KO mice. In step 13–16 spermatids, abnormal connecting pieces with incomplete segmented column and/or capitulum were frequently observed in KO mice but not in WT littermates. Bp, basal plate; CA, centriolar adjunct; An, annulus. Bars = 500 nm. **(E)** Schematic representation of the stepwise development of the connecting piece in WT (blue arrows) and FAM46C KO (red arrows) mice based on the TEM analyses. Red, Bp; dark green, Cp; light green, Sc; gray, Pc; black, An.

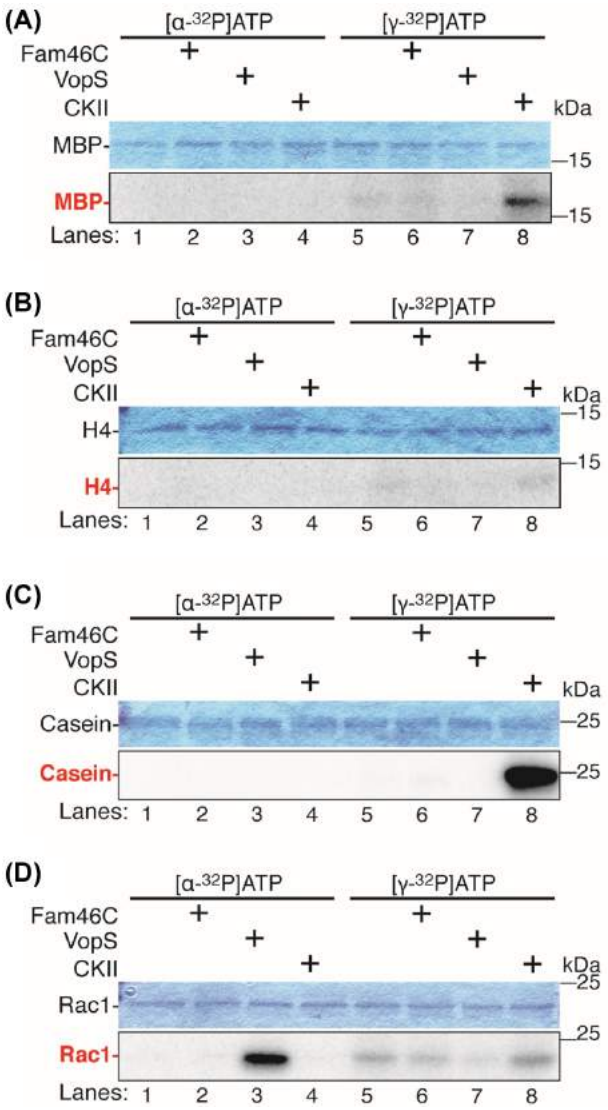


**Figure 4.** FAM46C does not AMPylate or phosphorylate general protein substrates. **(A)** Representative Coomassie gel and autoradiographs of AMPylation (lanes 1–4) and kinase (lanes 5–8) assays in which MBP was used as a substrate for 6xHIS-FAM46C (lanes 2 and 6), GST-VopSΔ30 (lanes 3 and 7), and Casein Kinase II. **(B)** Representative Coomassie gel and autoradiographs of AMPylation (lanes 1–4) and kinase (lanes 5–8) assays in which Histone H4 was used as a substrate for 6xHIS-FAM46C (lanes 2 and 6), GST-VopSΔ30 (lanes 3 and 7), and Casein Kinase II. **(C)** Representative Coomassie gel and autoradiographs of AMPylation (lanes 1–4) and kinase (lanes 5–8) assays in which Casein was used as a substrate for 6xHIS-FAM46C (lanes 2 and 6), GST-VopSΔ30 (lanes 3 and 7), and Casein Kinase II. **(D)** Representative Coomassie gel and autoradiographs of AMPylation (lanes 1–4) and kinase (lanes 5–8) assays in which 6xHIS-Rac1V12 (Rac1) was used as a substrate for 6xHIS-FAM46C (lanes 2 and 6), GST-VopSΔ30 (lanes 3 and 7), and Casein Kinase II.

incubated with the substrates myelin basic protein (MBP), histone H4, Casein, and Rac1 in the presence of [$\alpha^{32}$P]ATP or [$\gamma^{32}$P]ATP. As expected, VopS was able to AMPylate Rac1 (Figure 4A–D, lane 3), and Casein Kinase II was able to phosphorylate MBP and Casein with [$\gamma^{32}$P] ATP (Figure 4A, lane 8 and 4C, lane 8). However, FAM46C was unable to AMPylate (Figure 4A–D, lanes 2) or phosphorylate (Figure 4A–D, lanes 6) any of the generic substrates tested under these conditions. In addition, FAM46C was unable to undergo auto-AMPylation or auto-phosphorylation, a common characteristic of many active enzymes with these activities. Taken together, our data suggest that FAM46C is not a robust AMPylator or kinase; however, we cannot exclude the possibility that FAM46C, like other enzymes, such as VopS, may specifically target a distinct protein within the testis.

### Loss of function of FAM46C compromises sperm head fertilization ability

Previous studies showed that infertility of mice and humans with acephalic sperm caused by genetic mutation can be overcome by ICSI using the tailless sperm heads [26–28]. Therefore, we asked whether the tailless sperm head from FAM46C KO mice were fertile. We collected sperm heads from KO epididymides and injected them into WT oocytes and found that the rates of two-cell embryo and blastocyst development were significantly reduced using sperm heads of KO mice compared with those of WT mice; moreover, the rate of live offspring was further reduced when the 2-pronucleate embryos were transferred into the uteruses of recipient mice (21.9% in WT vs. 0.4% in KO) (Table 1A and B, Figure 5A and B).

We predicted that the reduction in live offspring production rate of FAM46C KO sperm heads was caused by abnormal DNA condensation or DNA damage. To test this hypothesis, we performed immuno-staining assays on adult testis sections to examine the expression of TNP2, a marker for chromatin condensation during spermiogenesis, but we did not detect any difference in nuclear condensation of spermatids between WT and KO mice (Figure 5C). However, the percentage of apoptotic sperm heads from the epididymides of the KO mice was 21.4%, while the percentage of apoptotic sperm heads of the WT mice was no more than 0.1% (Figure 5D). We also performed acridine orange test (AOT), which is a widely used method for assessing sperm DNA integrity [29], on the WT and KO sperm heads, and found that 22.8% of the KO sperm heads contained damaged DNAs, while the percentage of such sperm heads from WT mice was 1.0% (Figure 5E). Together, our data suggest that, unlike the results from other previous reports [26–28], sperm heads of FAM46C KO mice lose their fertilization ability probably due to apoptosis-induced DNA damage after sperm head-tail detachment, and this hypothesis warrants further investigations.

## Discussion

In this study, we report that FAM46C, a highly conserved non-canonical RNA polyadenylation polymerase, is localized to the manchette, a very specialized structure of spermatids. FAM46C KO mice have no obvious phenotype other than male infertility due to the production of acephalic sperm. A recent study provided evidence that FAM46C indeed possessed polyadenylation polymerase activity and that FAM46C KO mice had slight anemia, but it did not provide any results regarding the fertility of the KO mice [9]. Due to the highly specialized localization and function of FAM46C in mouse testes, we examined the potential of FAM46C as a protein kinase or AMPylator. Although we found no enzymatic activity in vitro, the regulatory role of FAM46C as an enzyme cannot be totally ruled out as this enzyme might have specific substrates.

Acephalic sperm is a rare type of sperm defects that have a genetic origin and that can be identified by morphological evaluations [30]. Although this disease has been well documented and described

**Table 1A.** In vitro development of oocytes injected with epididymal sperm heads from WT and FAM46C KO male mice.

| Sperm genotype | Total oocytes injected | 2PN (%, 2PN/total) | Two-cell embryos (%, two-cell embryos/2PN) | Blastocysts (%, blastocysts/two-cell embryos) |
|---|---|---|---|---|
| WT | 77 | 63 (81.8%) | 50 (79.4%) | 23 (46.0%) |
| KO | 72 | 60 (83.3%) | 13 (21.7%) | 2 (15.4%) |

2PN, 2-pronucleus embryo. For each genotype, the numbers of total oocytes injected and the subsequent stage embryos were pooled from two independent experiments (n = 2).

**Table 1B.** Birth rate of embryos from oocytes injected with epididymal sperm heads from WT and FAM46C KO male mice.

| Sperm genotype | 2PN | Recipients | Live offspring (%, offspring/2PN) | Offspring genotype |
|---|---|---|---|---|
| WT | 96 | 4 | 21 (21.9%) | FAM46C $^{+/+}$ |
| KO | 233 | 10 | 1 (0.4%) | FAM46C $^{+/-}$ |

2PN, 2-pronucleus embryo. For each genotype, the number of 2PN were pooled from four independent experiments (n = 4).

for years, recently two genes responsible for this condition in patients were reported, *SUN5* and *PMFBP1,* which encode SAD1 and UNC84 domain containing 5 and polyamine modulated factor 1 binding protein 1, respectively [27, 28, 31]. Importantly, in mice, several gene mutations that lead to acephalic sperm have been identified and these have been used to study the mechanisms of this disease [26, 27, 32–37]. These mouse models of acephalic sperm have revealed the complex nature of flagellar development. Most genetic defects result in not only the decoupling of sperm head and tail but also other abnormalities such as deformations of the nucleus, manchette, axoneme, and mitochondrial sheath. Intriguingly, major structural dynamics during spermatid development, such as manchette formation, nuclear condensation, and mitochondrial re-organization all appear normal in FAM46C KO mice. This is puzzling if FAM46C is expected to function in spermatids as a polyadenylation polymerase that may control transcript levels of many genes. Therefore, it is likely that FAM46C acts as a non-enzyme protein in spermatids. This idea is further supported by its lack of kinase or ampylation enzymatic activities, although these results need to be confirmed in the future by showing that the recombinant protein is active and by testing more substrates.

In terms of subcellular localization, the protein most similar to FAM46C is spermatogenesis-associated 6 (SPATA6). SPATA6 was identified as the first gene for which the murine KO resulted in almost 100% acephalic sperm [26]. SPATA6 is mainly expressed in the manchette in step 9–14 spermatids and is eventually confined to the connecting piece. The impaired development of the connecting piece was observed as early as at the beginning of step 9 spermatids of the SPATA6 KO mice, suggesting that a manchette-localized protein plays a role in the connecting piece formation. In this sense, FAM46C may also be involved in connecting piece development despite that it was only observed in the manchette. The interaction between SPATA6 and myosin suggests that SPATA6 may regulate myosin-based microfilament transport of proteins for flagellar development. Therefore, FAM46C may also play such a role, which warrants further investigation, and it will be instrumental to identify any interacting partner of FAM46C in the future.

Importantly, sperm heads from FAM46C KO mice lost almost all of its fertility as we only acquired one live mouse from 233 embryos derived from sperm head-injected oocytes, equivalent to a rate of 0.4% that is only 1.8% of the rate of WT mice. Several studies have claimed that healthy offspring were successfully derived from either mouse or human acephalic sperm heads through ICSI [26–28, 38]. However, of these studies, only two presented fertility rates [26, 38] whereas the rest only reported the birth of healthy offspring without any quantitative data [27, 28]. For the two studies with fertility rates reported, the ways by which sperm/sperm heads were collected and the methods by which fertility rates were calculated were different. For example, Yuan et al. (2015) collected sperm heads from epididymides and the rate was calculated by using the number of two-cell embryos as the denominator [26], whereas Fang et al. (2018) picked sperm with both heads and tails among mostly acephalic tails in semen to do ICSI and transferred only 3 good-quality embryos to the mother, all of which generated healthy babies [38]. We followed the way of Yuan et al. (2015) to collect epididymal sperm heads but used different criteria for fertility evaluation. Instead of using two-cell embryos to do embryo transfer and using its number as the denominator of the fertility rate, we directly transferred embryos at pronucleus stage to minimize the negative effect of longer in vitro duration after ICSI. Accordingly, we used the number of embryos at the pronucleus stage as the denominator of the fertility rate. However, even if we correct our fertility rate by the rate of two-cell embryos, the success rate is still only 1.5%, which compares poorly to the 26.3% of WT mice. These two numbers are lower than those from the *Spata6* mutant mice, which are 33.9% and 35.0% for KO and WT mice, respectively [26]. Therefore, our data strongly indicate that the sperm heads of FAM46C KO from the epididymides have lost their fertility by about 94.3%, and this is most likely due to apoptosis-induced DNA damages.

A very important observation in our study is that tailless sperm heads in the testis were very likely engulfed and digested by Sertoli cells. This observation, together with the low fertility rate of sperm heads from epididymides, has important clinical implications. We observed that genome-wide DNA damage was taking place in sperm heads either engulfed by Sertoli cells or in the epididymides, as revealed by TUNEL assays. We postulate that undetected DNA damage also occurs even if the sperm heads appears normal regardless of how they are collected. Genetic defects resulting from minor DNA damages can be passed to the next generation through ICSI. Although several studies emphasized successful births using acephalic sperm heads, safety concerns should not be ignored without long-term evaluations. At least, we should acknowledge that ICSI using acephalic sperm heads with different genetic origins is a case-by-case practice.

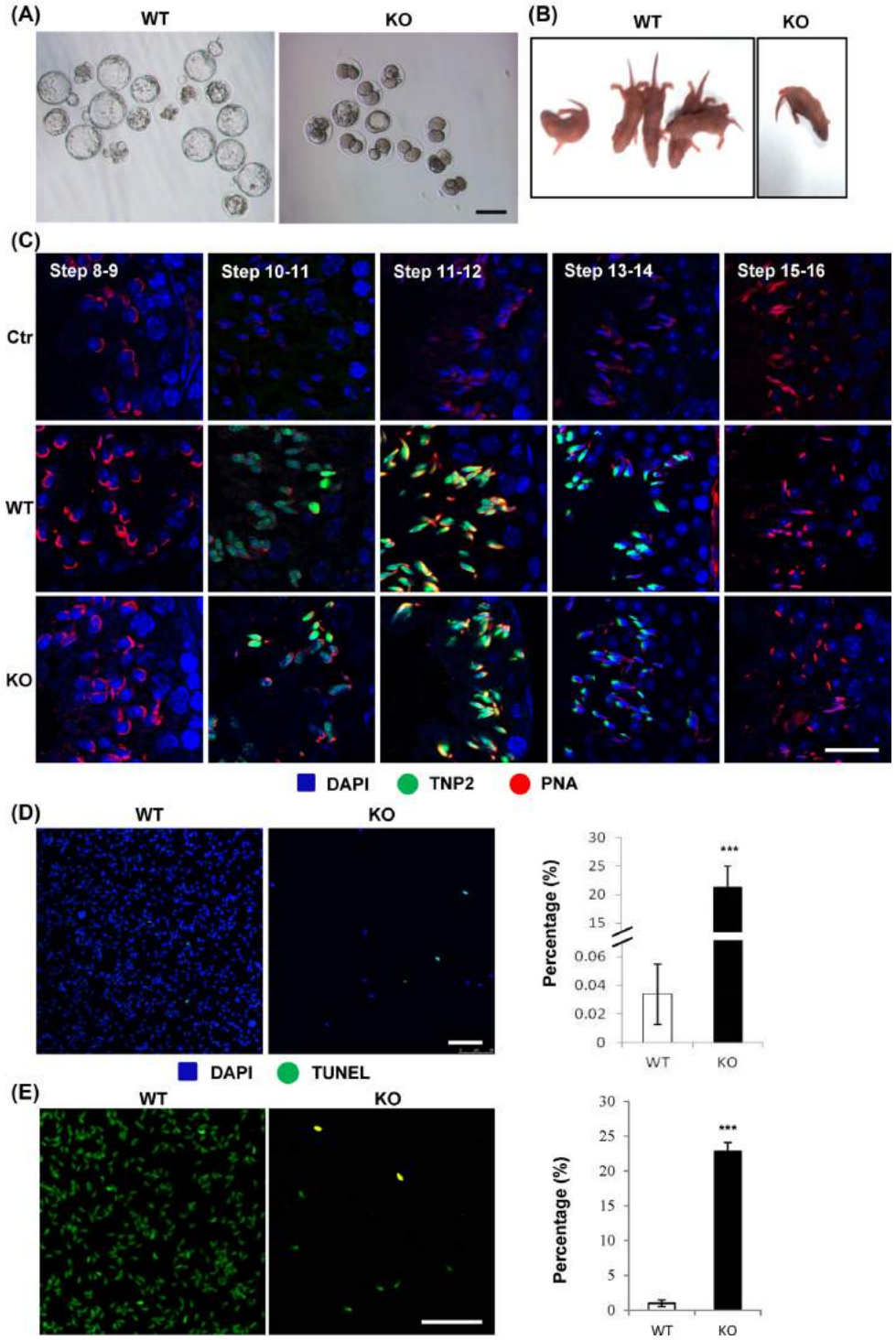


**Figure 5.** Evaluation of fertility, nuclear condensation, and apoptosis of sperm heads in epididymides. **(A)** Blastocyst development evaluation of embryos generated from WT and KO sperm heads using ICSI. Fewer blastocysts are observed for KO sperm heads than for WT sperm heads. Bars = 50 $\mu$m. **(B)** Offspring produced from ICSI embryos using sperm heads. **(C)** TNP2 immunostaining of testis sections from WT and KO mice. For TNP2 immunostaining, WT sections without primary antibody were used as negative controls (Ctr, top panel). Acrosomes were always revealed by rhodamine-PNA staining. Bars = 25 $\mu$m. **(D)** TUNEL assays on the sperm heads from the epididymides of WT and KO mice. At least 50 cells per sample were counted. (n = 4). Bars = 50 $\mu$m. **(E)** Acridine orange test (AOT) on epididymal spermatozoa collected from WT and KO mice. Green, normal sperm heads; Yellow/orange, sperm heads with DNA damages. At least 100 cells per sample were counted. (n = 3). Bars = 50 $\mu$m.

## Supplementary data

Supplementary data are available at *BIOLRE* online.

**Supplemental Figure S1.** Purity evaluations of the various isolated testicular cell types by quantitative real-time RT-PCR analyses of marker genes. The mRNA expression of zinc finger and BTB domain containing 16 (*Plzf*), KIT proto-oncogene receptor tyrosine kinase (*Kit*), stimulated by retinoic acid gene 8 (*Stra8*), synaptonemal complex protein 3 (*Sycp3*), protamine 2 (*Prm2*), and sperm maturation 1 (*Spem1*) was analyzed by quantitative RT-PCR. Data are presented as mean ± SEM, n = 4.

**Supplemental Figure S2.** Multiple sequence alignment of FAM46C proteins of 10 species showing that the protein is highly conserved during evolution.

**Supplemental Figure S3.** Characterization of FLAG-FAM46C KI mice model. (**A**) Litter sizes of KI/ + and KI/KI male mice. (n = 3). (**B**) Histological analyses of epididymis sections from WT and KI homozygous mice stained with HE. Bars = 25 $\mu$m. (**C**) HE staining of sperm released from epididymides showing that KI homozygous sperm are normal. Bars = 10 $\mu$m.

**Supplemental Figure S4.** Generation, genotyping and breeding of FAM46C KO mice. (**A**) Schematic illustration of FAM46C targeting by sgRNA using the CRISPR-Cas9 method. Single guide RNA was designed to target exon two. The triangle pair represents the primers used later in genotyping. Two founder mice were generated. One of the founder mice (FAM46C-39) contains a 39-bp deletion corresponding to 13 amino acids (aa) from aa 68–80 of the protein located in the NTase domain of FAM46C. The other one (FAM46C-1) has a single base deletion results in a truncated protein of 92 aa with 15 exogenous aa due to a frameshift. (**B**) Sequence confirmation of the mutated alleles of the two KO founders. (**C**) Breeding strategy for generating F2 KO, Het, and WT littermates from the first founder mouse. (**D**) Genotyping of F2 mice of the FAM46C-39 founder using genomic PCRs. PCR products of 149-bp and 110-bp represents the WT and mutant alleles, respectively. (**E–L**) Hematologic evaluations of concentration of blood hemoglobin (HGB) (**E**), hematocrit (HCT) in blood (**F**), red blood cells count (RBC) (**G**), mean corpuscular volume (MCV) (**H**), mean corpuscular hemoglobin (MCH) (**I**), mean corpuscular hemoglobin concentration (MCHC) (**J**), blood platelets (PLT) (**K**), and percentage of lymphocyte (LYM%) (**L**) from FAM46C WT and KO mice.

**Supplemental Figure S5.** Phenotypic characterization of FAM46C KO mice. (**A–B**) Quantitative comparison of body (**A**) and testis (**B**) weights among WT, Het, and KO mice. (n = 4). (**C**) PAS and hematoxylin staining of WT and KO testis sections. Bars = 25 $\mu$m. (**D**) SP56 immunostaining of stage VII–VIII seminiferous epithelia showed the acrosome was normal in KO mice. Bars = 25 $\mu$m. (**E–F**) HE-stained testis (**E**) and epididymis (**F**) sections from WT and the F2 offspring of the FAM46C-1 founder. Bars = 25 $\mu$m. (**G**) Litter sizes of WT, KO (FAM46C-1) male mice. (n = 3). (**H**) HE staining of sperm released from epididymis showing that KO (FAM46C-1) sperm are acephalic. Bars = 25 $\mu$m.

**Supplemental Figure S6.** Characterization of epididymal sperm released from or inside the epididymis. (**A**) HE staining of sperm released from the epididymis. Bars = 50 $\mu$m. (**B**) $\alpha$-TUBULIN and DAPI co-staining of epididymal sections of WT and KO mice. Bars = 25 $\mu$m.

**Supplemental Figure S7.** Localization of sperm heads of FAM46C KO mice in the testis. (**A**) PAS-staining of testis sections of KO mice showing sperm heads localized in the basal compartment of the tubules (black arrows). Bars = 50 $\mu$m. (**B**) TEM analyses of testis sections showing that the sperm heads are located inside Sertoli cells and close to the basement membrane. Bars = 2 $\mu$m. (**C**) TUNEL-positive and WT1-positive nuclei are adjacent to but not overlapping with each other. Bars = 25 $\mu$m. (**D**) WT1- and hematoxylin-stained testis sections of WT and KO mice. Sperm heads (black arrows) are adjacent to Sertoli cells in KO mice. Bars = 50 $\mu$m.

**Supplemental Table S1.** Oligonucleotides used in this study.

**Supplemental Table S2.** Antibodies used in this study.

**Supplemental Table S3.** mRNAs detected in testes of WT and KO mice.

## Acknowledgments

We thank Drs. Kim Orth and Amanda K. Casey from the University of Texas Southwestern Medical Center for their contributions in conducting the enzymatic assays of recombinant FAM46C. We thank Ms Yingzi Ma and Mr Pengyan Xia from the Institute of Zoology, Chinese Academy of Sciences for their help on TEM analyses. We thank Dr Shuguang Duo from the Institute of Zoology, Chinese Academy of Sciences, for his help on transgenic mice production.

**Conflict of Interest:** The authors declare no competing interests.

## References

1. Lin X, Han M, Cheng L, Chen J, Zhang Z, Shen T, Wang M, Wen B, Ni T, Han C. Expression dynamics, relationships, and transcriptional regulations of diverse transcripts in mouse spermatogenic cells. *RNA Biology* 2016; **13**:1011–1024.
2. Paronetto MP, Sette C. Role of RNA-binding proteins in mammalian spermatogenesis. *Int J Androl* 2010; **33**:2–12.
3. Gerstberger S, Hafner M, Tuschl T. A census of human RNA-binding proteins. *Nat Rev Genet* 2014; **15**:829–845.
4. Walker BA, Leone PE, Chiecchio L, Dickens NJ, Jenner MW, Boyd KD, Johnson DC, Gonzalez D, Dagrada GP, Protheroe RKM, Konn ZJ, Stockley DM et al. A compendium of myeloma-associated chromosomal copy number abnormalities and their prognostic value. *Blood* 2010; **116**:e56–e65.
5. Chapman MA, Lawrence MS, Keats JJ, Cibulskis K, Sougnez C, Schinzel AC, Harview CL, Brunet JP, Ahmann GJ, Adli M, Anderson KC, Ardlie KG et al. Initial genome sequencing and analysis of multiple myeloma. *Nature* 2011; **471**:467–472.
6. Boyd KD, Ross FM, Walker BA, Wardell CP, Tapper WJ, Chiecchio L, Dagrada G, Konn ZJ, Gregory WM, Jackson GH, Child JA, Davies FE et al. Mapping of chromosome 1p deletions in myeloma identifies FAM46C at 1p12 and CDKN2C at 1p32.3 as being genes in regions associated with adverse survival. *Clin Cancer Res* 2011; **17**:7776–7784.
7. Barbieri M, Manzoni M, Fabris S, Ciceri G, Todoerti K, Simeon V, Musto P, Cortelezzi A, Baldini L, Neri A, Lionetti M. Compendium of FAM46C gene mutations in plasma cell dyscrasias. *Br J Haematol* 2016; **174**:642–645.
8. Zhu YX, Shi CX, Bruins LA, Jedlowski P, Wang XW, Kortum KM, Luo ML, Ahmann JM, Braggio E, Stewart AK. Loss of FAM46C promotes cell survival in myeloma. *Cancer Res* 2017; **77**:4317–4327.
9. Mroczek S, Chlebowska J, Kulinski TM, Gewartowska O, Gruchota J, Cysewski D, Liudkovska V, Borsuk E, Nowis D, Dziembowski A. The non-canonical poly(A) polymerase FAM46C acts as an onco-suppressor in multiple myeloma. *Nat Commun* 2017; **8**:619.
10. Tanaka H, Kanda M, Shimizu D, Tanaka C, Kobayashi D, Hayashi M, Iwata N, Yamada S, Fujii T, Nakayama G, Sugimoto H, Fujiwara M et al. FAM46C serves as a predictor of hepatic recurrence in patients with resectable gastric cancer. *Ann Surg Oncol* 2017; **24**:3438–3445.
11. Zhang QY, Yue XQ, Jiang YP, Han T, Xin HL. FAM46C is critical for the anti-proliferation and pro-apoptotic effects of norcantharidin in hepatocellular carcinoma cells. *Sci Rep* 2017; **7**:396.

12. Wan XY, Zhai XF, Jiang YP, Han T, Zhang QY, Xin HL. Antimetastatic effects of norcantharidin on hepatocellular carcinoma cells by up-regulating FAM46C expression. *Am J Trans Res* 2017; **9**:155–166.
13. Fagerberg L, Hallstrom BM, Oksvold P, Kampf C, Djureinovic D, Odeberg J, Habuka M, Tahmasebpoor S, Danielsson A, Edlund K, Asplund A, Sjostedt E et al. Analysis of the human tissue-specific expression by genome-wide integration of transcriptomics and antibody-based proteomics. *Mol Cell Proteomics* 2014; **13**:397–406.
14. Yue F, Cheng Y, Breschi A, Vierstra J, Wu WS, Ryba T, Sandstrom R, Ma ZH, Davis C, Pope BD, Shen Y, Pervouchine DD et al. A comparative encyclopedia of DNA elements in the mouse genome. *Nature* 2014; **515**:355–364.
15. Gan HY, Wen L, Liao SY, Lin XW, Ma TT, Liu J, Song CX, Wang M, He C, Han CS, Tang FC. Dynamics of 5-hydroxymethylcytosine during mouse spermatogenesis. *Nat Commun* 2013; **4**:1995.
16. Kuchta K, Knizewski L, Wyrwicz LS, Rychlewski L, Ginalski K. Comprehensive classification of nucleotidyltransferase fold proteins: identification of novel families and their representatives in human. *Nucleic Acids Res* 2009; **37**:7701–7714.
17. Kuchta K, Muszewska A, Knizewski L, Steczkiewicz K, Wyrwicz LS, Pawlowski K, Rychlewski L, Ginalski K. FAM46 proteins are novel eukaryotic non-canonical poly(A) polymerases. *Nucleic Acids Res* 2016; **44**:3534–3548.
18. Shen B, Zhang J, Wu HY, Wang JY, Ma K, Li Z, Zhang XG, Zhang PM, Huang XX. Generation of gene-modified mice via Cas9/RNA-mediated gene targeting. *Cell Res* 2013; **23**:720–723.
19. Gan HY, Lin XW, Zhang ZQ, Zhang W, Liao SY, Wang LX, Han CS. piRNA profiling during specific stages of mouse spermatogenesis. *RNA* 2011; **17**:1191–1203.
20. Chen Q, Peng HY, Lei L, Zhang Y, Kuang HB, Cao YJ, Shi QX, Ma TH, Duan EK. Aquaporin3 is a sperm water channel essential for postcopulatory sperm osmoadaptation and migration. *Cell Res* 2011; **21**:922–933.
21. Yarbrough ML, Li Y, Kinch LN, Grishin NV, Ball HL, Orth K. AMPylation of Rho GTPases by vibrio VopS disrupts effector binding and downstream signaling. *Science* 2009; **323**:269–272.
22. Grammel M, Luong P, Orth K, Hang HC. A chemical reporter for protein AMPylation. *J Am Chem Soc* 2011; **133**:17103–17105.
23. Nakata H, Wakayama T, Asano T, Nishiuchi T, Iseki S. Identification of sperm equatorial segment protein 1 in the acrosome as the primary binding target of peanut agglutinin (PNA) in the mouse testis. *Histochem Cell Biol* 2017; **147**:27–38.
24. Lehti MS, Sironen A. Formation and function of the manchette and flagellum during spermatogenesis. *Reproduction* 2016; **151**:R43–R54.
25. Lehti MS, Sironen A. Formation and function of sperm tail structures in association with sperm motility defects. *Biol Reprod* 2017; **97**:522–536.
26. Yuan SQ, Stratton CJ, Bao JQ, Zheng HL, Bhetwal BP, Yanagimachi R, Yan W. Spata6 is required for normal assembly of the sperm connecting piece and tight head-tail conjunction. *Proc Natl Acad Sci USA* 2015; **112**:E430–E439.
27. Shang YL, Zhu FX, Wang LN, Ouyang YC, Dong MZ, Liu C, Zhao HC, Cui XH, Ma DY, Zhang ZG, Yang XY, Guo YS et al. Essential role for SUN5 in anchoring sperm head to the tail. *Elife* 2017; **6**:e28199.
28. Zhu FX, Liu C, Wang FS, Yang XY, Zhang JJ, Wu H, Zhang ZG, He XJ, Zhang Z, Zhou P, Wei ZL, Shang YL et al. Mutations in PMFBP1 cause acephalic spermatozoa syndrome. *Am J Hum Genet* 2018; **103**:188–199.
29. Evenson DP. The Sperm Chromatin Structure Assay (SCSAÂ®) and other sperm DNA fragmentation tests for evaluation of sperm nuclear DNA integrity as related to fertility. *Anim Reprod Sci* 2016; **169**:56–75.
30. Chemes HE, Puigdomenech ET, Carizza C, Olmedo SB, Zanchetti F, Hermes R. Acephalic spermatozoa and abnormal development of the head-neck attachment: a human syndrome of genetic origin. *Hum Reprod* 1999; **14**:1811–1818.
31. Zhu FX, Wang FS, Yang XY, Zhang JJ, Wu H, Zhang Z, Zhang ZG, He XJ, Zhou P, Wei ZL, Gecz J, Cao YX. Biallelic SUN5 mutations cause autosomal-recessive acephalic spermatozoa syndrome. *Am J Hum Genet* 2016; **99**:1405–1405.
32. Mendoza-Lujambio I, Burfeind P, Dixkens C, Meinhardt A, Hoyer-Fender S, Engel W, Neesen J. The Hook1 gene is non-functional in the abnormal spermatozoon head shape (azh) mutant mouse. *Hum Mol Genet* 2002; **11**:1647–1658.
33. Netzel-Arnett S, Bugge TH, Hess RA, Carnes K, Stringer BW, Scarman AL, Hooper JD, Tonks ID, Kay GF, Antalis TM. The glycosylphosphatidylinositol-anchored serine protease PRSS21 (testisin) imparts murine epididymal sperm cell maturation and fertilizing ability1. *Biol Reprod* 2009; **81**:921–932.
34. Tokuhiro K, Isotani A, Yokota S, Yano Y, Oshio S, Hirose M, Wada M, Fujita K, Ogawa Y, Okabe M, Nishimune Y, Tanaka H. OAZ-t/OAZ3 is essential for rigid connection of sperm tails to heads in mouse. *PLoS Genet* 2009; **5**: e1000712.
35. Liska F, Gosele C, Rivkin E, Tres L, Cardoso MC, Domaing P, Krejci E, Snajdr P, Lee-Kirsch MA, de Rooij DG, Kren V, Krenova D et al. Rat hd mutation reveals an essential role of centrobin in spermatid head shaping and assembly of the head-tail coupling apparatus. *Biol Reprod* 2009; **81**:1196–1205.
36. Kierszenbaum AL, Rivkin E, Tres LL, Yoder BK, Haycraft CJ, Bornens M, Rios RM. GMAP210 and IFT88 are present in the spermatid golgi apparatus and participate in the development of the acrosome-acroplaxome Complex. *Dev Dynam* 2011; **240**:723–736.
37. Yang KF, Meinhardt A, Zhang B, Grzmil P, Adham IM, Hoyer-Fender S. The small heat shock protein ODF1/HSPB10 is essential for tight linkage of sperm head to tail and male fertility in mice. *Mol Cell Biol* 2012; **32**:216–225.
38. Fang JZ, Zhang JJ, Zhu FX, Yang XY, Cui YG, Liu JY. Patients with acephalic spermatozoa syndrome linked to SUN5 mutations have a favorable pregnancy outcome from ICSI. *Hum Reprod* 2018; **33**:372–377.